JOURNAL OF AIRCRAFT
Vol. 43, No. 3, May–June 2006

Unified Aeroelastic and Flight Dynamic Formulation via Rational Function Approximations

Dario H. Baldelli* and P. C. Chen†
ZONA Technology, Scottsdale, Arizona 85258
and
Jose Panza‡
General Atomics–Aeronautical Systems, San Diego, California 92127

A unified aeroelastic and flight dynamic formulation is sought to take into account the influence of aeroelastic effects on the flight dynamic behavior of the whole aircraft in a format fully compatible with the aeroelastic, flight dynamics, and automatic control disciplines. By allowing the inclusion of gravity-related terms, vertical acceleration–related aerodynamic stability derivatives, and lift and drag forces due to forward-velocity perturbations into the rational function approximation matrices, the traditional quasi-steady flight dynamic equations of motion are fully recovered. Closed-form solutions are presented for translational and rotational degrees of freedom in the aeroelastic model. The General Atomics–Aeronautical Systems (GA-ASI) Predator® unmanned aerial vehicle is used to numerically demonstrate the unified aeroelastic modeling framework. The results indicate that this approach reproduces, with a high degree of fidelity, the underlying quasi-steady flight dynamic model when no elastic modes are included in the aeroelastic model. Comments are provided to determine the approximate number of elastic modes that need to be included in the aeroelastic model to accurately model its flight dynamic behavior.

Nomenclature

$[A_i]$	=	aerodynamic-force matrix
b	=	aircraft wing span
$[C]$	=	structural-damping matrix
c	=	reference chord
g	=	gravity acceleration
$[K]$	=	structural-stiffness matrix
k	=	reduced frequency, $\omega c/2V_\infty$
$[M]$	=	mass-structural matrix
$\{P\}$	=	vector of gravity-related components
p	=	nondimensional Laplace variable, sL/V_∞
$[Q]$	=	generalized aerodynamic matrix force
$[R]$	=	diagonal aerodynamic root matrix
s	=	Laplace variable
$[T_A]$	=	body-to-stability-axes transformation matrix
V_∞	=	aircraft airspeed
$\{\delta_c\}$	=	vector of control-surface deflections
$\{\xi\}$	=	vector of generalized structural displacements
ω	=	frequency of oscillation

Subscripts

a	=	related to aerodynamic lag
ae	=	related to aeroelastic plant
c	=	related to control commands
i	=	0,1,2 related to quasi-steady-model approximation
lat	=	related to lateral dynamics plane
long	=	related to longitudinal dynamics plane
R	=	related to rigid-body states
s	=	related to structural deflections

Received 14 March 2005; accepted for publication 6 September 2005.

*Control Engineering Specialist. Member AIAA.
†Vice President. Member AIAA.
‡Structural Analysis Group Manager. Member AIAA.

I. Introduction

THIS paper deals with an unified aeroelastic formulation to take into account the influence of aeroelastic effects on the flight dynamic behavior of the whole aircraft. Linear-flutter engineering models that incorporate translational and rotational rigid-body degrees of freedom are not able to recover the traditional flight dynamic equations of motion because of the inherent conflicting modeling objectives. Among them, the finite-element-model coordinate system, the unsteady modeling of the aerodynamic forces using pure harmonic motion, and the missing gravity-related terms in the aeroelastic formulation can be held accountable for the differences observed in the eigenvalues associated with the free longitudinal and lateral dynamic modes. Traditionally, the aircraft rigid-body behaviors, such as the short period, phugoid, and Dutch roll, among others, have been described using quasi-steady aerodynamic forces, whereas the aeroelastic stability behavior is completely characterized by unsteady aerodynamic forces.[1] Therefore, it would be desirable to develop a single modeling capability to deal with translational and/or rotational rigid-body modes as well as elastic modes in a format fully compatible with aeroelastic, flight dynamics, and automatic control disciplines.

In the past, several techniques were developed to systematically incorporate aeroelastic effects into the aircraft dynamic equations of motion. Among these, Rodden and Love[2] addressed the conservation of the angular-momentum issue, and Whinter et al.[3,4] and Dykman and Rodden[5] formulated the p-transform approach to generate reduced-order models that avoid additional state variables to represent the unsteady aerodynamics.

In this work, we intend to further extend the findings of Refs. 4 and 5 by proposing unified aeroelastic formulation to take into account the influence of aeroelastic effects on the translational and rotational rigid-body modes of the aircraft. Here, the rational function approximation (RFA) setup usually sought to model the unsteady aerodynamic forces computed for purely oscillatory motion can be dually considered as the aeroelastician's natural tool to recover the quasi-steady longitudinal and lateral equations of motion ordinarily used by the flight control engineer.

To this end, this unified modeling framework will be composed of the following main tasks: 1) coordinate transformations between the principle axes and the flight dynamic's stability axes,[2] 2) incorporate measured aerodynamic stability derivatives from wind-tunnel or

flight tests[6,7] into the RFA matrices, and 3) include the gravity-related components as well as lift and drag forces due to forward-velocity perturbations within the aeroelastic formulation.

The last step constitutes the main contribution of this work, leading to an accurate recovery of the phugoid, spiral and roll-subsidence dynamic modes that appear in the flight dynamic description of the aircraft. Its implementation will naturally extend the RFA setup into a flight dynamic–oriented class.

We hope this modeling framework will become an enabling tool among the aeroelastic, flight dynamics, and flight control disciplines by providing a common state–space representation that accurately models the influence of the elastic modes on the translational and rotational rigid-body modes of the whole aircraft.

The outline of the paper is as follows. In Sec. II, the standard time-domain aeroelastic representation is briefly described. Section III presents the transformation between principle and stability axes. Section IV delineates how to update the quasi-steady aerodynamic part of the unsteady aerodynamic model and also how to include the gravity- and acceleration-related terms into the RFA setup. In Sec. V, the quasi-steady longitudinal and lateral dynamics closed-form solutions in the absence of elastic modes are computed. Finally in Sec. VI, the GA-ASI Predator[8] unmanned aerial vehicle (UAV) example is given to illustrate the application of the unified aeroelastic formulation. The Predator represents an actual state-of-the-art UAV, validated using production flutter engineering tools.[9] A summary is provided in Sec. VII.

II. Time-Domain Aeroelastic Formulation

It is well known that aeroelasticity can be viewed as a feedback interaction mechanism between structural dynamics and the unsteady aerodynamic forces. The former is induced by the static or dynamic deformation of the structure and the flight parameters (i.e., Mach number and altitude). This aerodynamic feedback mechanism modifies the rigid-body and vibration modes that characterize the dynamic behavior of the aircraft.[1]

In what follows, the time-domain aeroelastic formulation is briefly described closely following Karpel,[10] and it will be used to identify the key enabling elements involved in the recovering process of the traditional flight dynamic equations of motion[11] from the more general aeroelastic framework.

Let's consider the aeroelastic equation of motion in generalized coordinates, excited by control-surface motion and inertial loads at a given dynamic pressure q_∞,

$$[M_s]\{\ddot{\xi}\} + [C_s]\{\dot{\xi}\} + [K_s]\{\xi\} + q_\infty[Q_s(p)]\{\xi\} = -([M_c]\{\ddot{\delta}_c\} + q_\infty[Q_s(p)]\{\dot{\delta}_c\}) + \{P\} \tag{1}$$

where $[M_s] \in \mathbb{R}^{n_s \times n_s}$, $[C_s] \in \mathbb{R}^{n_s \times n_s}$, and $[K_s] \in \mathbb{R}^{n_s \times n_s}$ are the generalized mass, damping, and stiffness matrices, $[M_c] \in \mathbb{R}^{n_c \times n_c}$ is the coupling mass matrix between the control and the structural modes, $\{\xi\} \in \mathbb{R}^{n_s}$ is the vector of generalized structural deflections including the rigid-body modes, and $\{\delta_c\} \in \mathbb{R}^{n_c}$ is the vector of control-surface-commanded deflections. In addition, $[Q_s] \in \mathbb{R}^{n_s \times n_s}$ and $[Q_c] \in \mathbb{R}^{n_c \times n_c}$ are the generalized unsteady aerodynamic-force coefficient matrices associated with the structural and control modes, and $\{P\} \in \mathbb{R}^{n_s}$ is related to the weight components through the Euler angles θ and ϕ,[7]

$$\{P\} = [\Phi]^T[M]\begin{bmatrix} I_3 \\ I_3 \\ I_3 \\ \vdots \end{bmatrix}\begin{Bmatrix} -g\sin\theta \\ g\cos\theta\sin\phi \\ g\sin\theta\cos\phi \end{Bmatrix} \tag{2}$$

where $[\Phi]^T \in \mathbb{R}^{n_s \times m}$, $[M] \in \mathbb{R}^{m \times m}$, and $I_3 \in \mathbb{R}^{3\times 3}$ are the modal matrix, the mass matrix in physical coordinates, and the identity matrix, respectively, m is the number of degree of freedom of the finite element method (FEM) model, and g is acceleration due to the gravity, respectively. The most general RFA to the aerodynamic-force coefficient matrix is

$$[Q(p)] = [A_o] + [A_1]p + [A_2]p^2 + [D](p[I] - [R])^{-1}[E]p \tag{3}$$

where $p = sc/2V_\infty$ is the nondimensional Laplace variable, s is the Laplace variable, c is the reference chord, and V_∞ is the true airspeed. The aerodynamic data is computed for pure harmonic oscillations in the imaginary axis, and by the analytic continuity principle their domain of application is extended to the whole complex plane. The approximation process involves the replacement of p by ik, where k is the nondimensional frequency $k = \omega c/2V_\infty$.

The least-square procedures are used to compute the matrix approximation coefficients $[A_i] \in \mathbb{R}^{n\times n}$; $i = 0,\ 1,\ 2$; $[D] \in \mathbb{R}^{n \times n_a}$; $[R] \in \mathbb{R}^{n_a \times n_a}$; and $[E] \in \mathbb{R}^{n_a \times n}$, where $n = n_s + n_c$ is the number of total elastic modes composed from structural and control modes, and n_a is the number of aerodynamic lag terms. Note that Eq. (3) can handle both Roger[12] and minimum-state[13] formulations to fit the tabulated $[Q(ik)]$ matrices. In general, the $[A_i]$ and $[E]$ matrices are column partitioned as

$$[A_i] = \begin{bmatrix} A_{s_i} & A_{c_i} \end{bmatrix}, \qquad i = 0, 1, 2$$

$$[E] = [E_s \ \ E_c] \tag{4}$$

In this formulation, the $[A_i]$, $i = 0, 1, 2$, coefficient matrices represent the quasi-steady aerodynamic forces by playing the roles of an equivalent aerodynamic stiffness, aerodynamic damping, and aerodynamic inertia, and the remnant terms are used to model the flow unsteadiness by Padé approximants. These effects can be modeled as a state-space realization,

$$\{\dot{x}_a\} = \begin{bmatrix} E_s \vdots E_c \end{bmatrix}\begin{Bmatrix} \dot{\xi} \\ \dot{\delta}_c \end{Bmatrix} + (V_\infty/b)[R]\{x_a\}, \qquad \{z_a\} = [D]\{x_a\} \tag{5}$$

where x_a is the aerodynamic vector state. Substituting Eqs. (3) and (5) into Eq. (1), while considering p, will allow the overall open-loop aeroelastic system with external excitation for a fixed flight condition to be written in state-space form as

$$\begin{Bmatrix} \dot{\xi} \\ \ddot{\xi} \\ \dot{x}_a \end{Bmatrix} = \underbrace{\begin{bmatrix} 0 & I & 0 \\ \bar{K}_s & \bar{C}_s & \bar{D} \\ 0 & E_s & \bar{R} \end{bmatrix}}_{A_{\text{ae}}}\begin{Bmatrix} \xi \\ \dot{\xi} \\ x_a \end{Bmatrix} + \underbrace{\begin{bmatrix} 0 & 0 & 0 \\ \bar{K}_c & \bar{C}_c & \bar{M}_c \\ 0 & E_c & 0 \end{bmatrix}}_{B_{\text{ae}}}\begin{Bmatrix} \delta_c \\ \dot{\delta}_c \\ \ddot{\delta}_c \end{Bmatrix} + \begin{bmatrix} 0 \\ \bar{M}P \\ 0 \end{bmatrix} \tag{6}$$

or in a more compact form,

$$\{\dot{x}_{\text{ae}}\} = [A_{\text{ae}}]\{x_{\text{ae}}\} + [B_{\text{ae}}]\{u\} + \{w\} \tag{7}$$

where

$$x_{\text{ae}}^T = \begin{Bmatrix} \xi^T & \dot{\xi}^T & x_a^T \end{Bmatrix}^T, \qquad u^T = \begin{Bmatrix} \delta_c^T & \dot{\delta}_c^T & \ddot{\delta}_c^T \end{Bmatrix}^T$$

$$w^T = \{0^T \ \ (\bar{M}P)^T \ \ 0^T\}^T$$

and

$$\bar{M} = \left[[M_s] + \left(q_\infty b^2/V_\infty^2\right)\left[A_{s_2}\right]\right]^{-1}$$

$$\bar{K}_s = -\bar{M}\left[[K_s] + q_\infty\left[A_{s_o}\right]\right]$$

$$\bar{C}_s = -\bar{M}\left[[C_s] + (q_\infty b/V_\infty)\left[A_{s_1}\right]\right]$$

$$\bar{M}_c = -\bar{M}\left[[M_c] + \left(q_\infty b^2/V_\infty^2\right)\left[A_{c_2}\right]\right], \qquad \bar{K}_c = -q_\infty\bar{M}\left[A_{c_o}\right]$$

$$\bar{C}_c = -(q_\infty b/V_\infty)\bar{M}\left[A_{c_1}\right], \qquad \bar{D} = q_\infty\bar{M}[D]$$

$$\bar{R} = (V_\infty/b)[R]$$

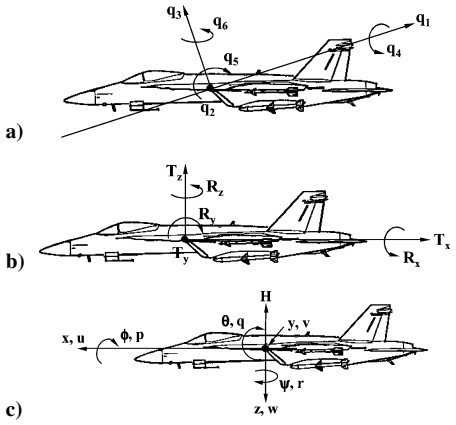

Fig. 1 Coordinate transformations.

Equation (6) mathematically describes the feedback mechanism between the structural dynamics and the unsteady aerodynamic model. It is observed that by eliminating all the terms related to the aerodynamic lag states, that is, the last row and column in the $[A_{ae}]$ and $[B_{ae}]$ matrices (shadowed areas), the traditional flight dynamic equations of motion can presumably be recovered. Otherwise, the inclusion of the dynamic model for the unsteady aerodynamic forces will result in a full aeroelastic system.

Thus, to fully recover the flight dynamic equations of motion, a twofold transformation process of the aeroelastic modeling framework is proposed. First, it involves a coordinate-axes transformation to change the structural modes into airframe states, enabling the well-known separation principle between the longitudinal and lateral dynamics. Second, it identifies the location of key enabling terms within the unsteady aerodynamic model. The former is an accepted practice using production flutter engineering tools,[3–5,9] whereas the latter is implemented by the proper allocation of the gravity components vector w as and the lift and drag force terms related to forward-velocity perturbations within the RFA setup.

III. Transformation Between Principle and Stability Axes

The objective of the transformation process is to change the structural rigid-body modes into the airframe states so that the rigid-body submatrices in the state–space equations of the aeroelastic system have the same definition as those of the flight dynamics discipline. Figure 1 shows the two-stage procedure for such transformation. It can be summarized as follows:

1. Principle axes to body axes, Fig. 1a to b: The generalized coordinates of the six rigid-body modes computed by the structural FEM are usually defined in the principle axis. Following Ref. 3, the transformation from the principle axes $\{x_q\}$ to the body axes $\{\xi_R\}$ is performed through the generic matrices $[R_P]$ and $[R_B]$[9]:

$$\{x_q\}^T = \{q_1, q_2, \ldots, q_6\}^T \tag{8}$$

$$\{\xi_R\}^T = \{T_x, T_y, T_z, R_x, R_y, R_z\}^T \tag{9}$$

$$\{x_q\} = [R_P]^{-1}[R_B]\{\xi_R\} \tag{10}$$

where $[R_P]$ is the rigid-body modal matrix in the principle axis and $[R_B]$ is the rigid-body modal matrix in the body axis at the c.g. location, respectively.

In Eq. (9), T_x is the fore–aft rigid-body mode, T_y is the lateral translational rigid-body mode, and T_z is the plunge rigid-body mode. In addition, R_x is the roll rigid-body mode, R_y is the pitch rigid-body mode, and R_z is the yaw rigid-body mode. It should be noted that after the transformation the generalized mass matrix, $[M_s]$ is no longer necessarily diagonal. In fact, the submatrix associated with the rigid-body modes is identical to the mass matrix in the flight dynamics equation; that is, the off-diagonal terms contain the products of inertia,

$$[M_s] = \left[\begin{array}{c|c} M_{rb} & 0 \\ \hline 0 & M_{ee} \end{array}\right]$$

where the $[M_{rb}]$ and $[M_{ee}]$ matrices are defined as

$$[M_{rb}] = \begin{bmatrix} m & 0 & 0 & 0 & 0 & 0 \\ 0 & m & 0 & 0 & 0 & 0 \\ 0 & 0 & m & 0 & 0 & 0 \\ 0 & 0 & 0 & I_{xx} & 0 & I_{xz} \\ 0 & 0 & 0 & 0 & I_{yy} & 0 \\ 0 & 0 & 0 & I_{xz} & 0 & I_{zz} \end{bmatrix}$$

$$[M_{ee}] = \begin{bmatrix} \ddots & & & & & \\ & \ddots & & & & \\ & & m_{ii} & & & \\ & & & \ddots & & \\ & & & & \ddots & \end{bmatrix}$$

where $m, m_{ii}, I_{xx}, I_{yy}, I_{zz}$, and I_{xz} are the mass of the whole aircraft; the generalized mass associated with the iith elastic mode; the roll, pitch, and yaw moments of inertia; and the lateral/directional products of inertia, respectively.

2. Body axes to stability axes, Fig. 1b to c: In this stage, the transformation from the body axes $\{\xi_R\}$ to the airframe axes $\{\xi_{AS}\}$ is performed through the matrix $[T_A]$:

$$\{\xi_R\}^T = \{T_x, T_y, T_z, R_x, R_y, R_z\}^T \tag{11}$$

$$\begin{Bmatrix} \xi_R \\ \dot{\xi}_R \end{Bmatrix} = [T_A]\{\xi_{AS}\} \tag{12}$$

$$\{\xi_{AS}\}^T = \{x, y, u, \beta, h, p, w, r, \theta, \phi, q, \psi\}^T \tag{13}$$

where $x, y, u, \beta, h, p, w, r, \theta, \phi, q$, and ψ are the perturbed quantities related to the forward position, lateral position, forward airspeed, sideslip angle, altitude, roll rate, upward velocity, yaw rate, Euler pitch angle, Euler roll angle, pitch rate, and Euler azimuth angle, respectively. These are the main perturbed variables that describe the aircraft behavior in the stability axes system. For a symmetric maneuver, Refs. 3 and 4 described the matrix $[T_A]_{long}$ as follows:

$$\begin{Bmatrix} T_x \\ T_z \\ R_y \\ \dot{T}_x \\ \dot{T}_z \\ \dot{R}_y \end{Bmatrix} = \begin{bmatrix} -1 & 0 & 0 & 0 & 0 & 0 \\ 0 & 0 & 1 & 0 & 0 & 0 \\ 0 & 0 & 0 & 0 & 1 & 0 \\ 0 & -1 & 0 & 0 & 0 & 0 \\ 0 & 0 & 0 & -V_\infty & V_\infty & 0 \\ 0 & 0 & 0 & 0 & 0 & 1 \end{bmatrix} \begin{Bmatrix} x \\ u \\ h \\ \alpha \\ \theta \\ q \end{Bmatrix} \tag{14}$$

If w is selected (instead of α), $\dot{T}_z$ is modified as $\dot{T}_z = -w + V_\infty\theta$. Additionally, this work further extends the approach delineated in Ref. 4 for the antisymmetric maneuvers. In this case, the matrix $[T_A]_{lat}$ is defined as follows:

$$\begin{Bmatrix} T_y \\ R_x \\ R_z \\ \dot{T}_y \\ \dot{R}_x \\ \dot{R}_z \end{Bmatrix} = \begin{bmatrix} 1 & 0 & 0 & 0 & 0 & 0 \\ 0 & 0 & 0 & 0 & -1 & 0 \\ 0 & 0 & 0 & 0 & 0 & -1 \\ 0 & V_\infty & 0 & 0 & 0 & V_\infty \\ 0 & 0 & -1 & 0 & 0 & 0 \\ 0 & 0 & 0 & -1 & 0 & 0 \end{bmatrix} \begin{Bmatrix} y \\ \beta \\ p \\ r \\ \phi \\ \psi \end{Bmatrix} \tag{15}$$

If v is selected (instead of β), $\dot{T}_y$ is modified as $\dot{T}_y = v + V_\infty\psi$.

Finally, for an asymmetric maneuver, the matrix $[T_A] \in \mathbb{R}^{12\times 12}$ will be composed of the proper distribution of the elements that form the rows and columns of the $[T_A]_{\text{long}}$ and $[T_A]_{\text{lat}}$matrices. Therefore, a seamless axes transformation process can be performed to convert the rigid-body modes from the production finite-element codes to the airframe states in the airframe stability axes system.

IV. Rational Function Approximation Setup: Updating the Quasi-Steady Aerodynamic Model and Including Gravity Terms

In this section, the rational function approximation concept is further extended to become the aeroelastician's natural tool for flight dynamic modeling purposes. By allowing the inclusion of gravity-related components, vertical acceleration–related aerodynamic stability derivatives, and the lift and drag forces due to forward-velocity perturbations, the traditional quasi-steady flight dynamic equations of motion will be fully recovered. A straightforward procedure is outlined to identify the location of the elements that need to be updated/replaced within the quasi-steady aerodynamic matrices, that is, $[A_0]$, $[A_1]$, and $[A_2]$ of Eq. (3).

In general, production flutter engineering tools employ panel methods to compute linear unsteady aerodynamics. However, the drag-related stability derivatives computed by those methods, such as C_{D_α} and C_{D_q} among others, are not accurate enough because of the inherent lack of skin friction drag. Hence, it will be particularly useful to replace the computed translational and rotational rigid-body-related elements at zero and/or low reduced frequency in the generalized aerodynamic stiffness and damping matrices, $[A_0]$ and $[A_1]$, with wind-tunnel- and/or flight-test-measured aerodynamic stability derivatives.[7]

For instance, at zero reduced frequency ($p=0$), the RFA model is reduce to $[Q(0)]=[A_0]$, which contains elements associated with the static aerodynamic stability derivatives, if rigid-body modes exist. Specifically, for symmetric structural modes, namely the fore–aft mode, plunge mode, and pitch mode, the static aerodynamics associated with these three rigid-body modes are located in the $[A_0]$ matrix as shown in Fig. 2, where a_{11}, a_{21}, and a_{31} are the aerodynamics forces due to the fore–aft mode and a_{12}, a_{22}, and a_{32} are due to the plunge mode. At zero reduced frequency, all of these terms are normally zero because the fore–aft and the plunge modes cannot introduce an angle of attack. The a_{13}, a_{23} and a_{33} are the unsteady aerodynamics coefficients due to the pitch mode. In fact, at zero reduced frequency, they can be directly correlated with the longitudinal static aerodynamic stability derivatives D_α, L_α, and M_α (i.e., the dimensional induced drag force, lift force, and pitch moment at unit angle of attack (in radians) of the whole configuration), as shown in Eq. (16):

$$a_{13} = -0.5(D_\alpha/q_\infty), \qquad a_{23} = -0.5(L_\alpha/q_\infty)$$
$$a_{33} = -0.5(M_\alpha/q_\infty) \tag{16}$$

where the negative sign in these equations is due to the sign convention uses for $[Q(p)]$ in Zona AEROelastic Software System

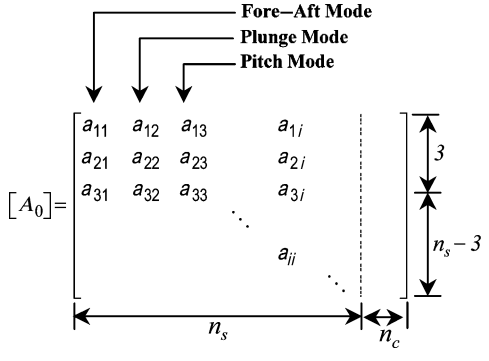

Fig. 2 Rigid-body modes location inside $[A_0]$.

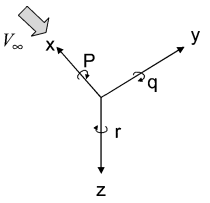

a) Stability axes

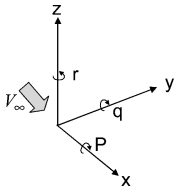

b) ZAERO's aerodynamic coordinates

Fig. 3 Aerodynamic coordinate systems.

(ZAERO).[9] Figure 3 shows the x, y, and z axes of the stability axis and the ZAERO system of aerodynamic coordinates.

The terms a_{1i}, a_{2i}, a_{3i} and a_{ii} shown in Eq. (15) represent the unsteady aerodynamics due to the ith structural mode. If this ith structural mode is a control surface mode, then they can be replaced by the wind-tunnel-measured aerodynamic stability derivatives of the control surface, where a_{1i}, a_{2i}, and a_{3i} can be correlated with the drag, lift, and moment stability derivatives due to control surface deflection, respectively, whereas a_{ii} is its own control surface hinge moment.

In general, the related symmetric rigid-body modes submatrices in $[A_{s_0}]$ and $[A_{s_1}]$ can be expressed as a function of the following longitudinal static and damping nondimensional aerodynamic stability derivatives,

$$\left[A_{s_0}\right]_{\text{sym}} = \begin{bmatrix} 0 & 0 & -S\left(C_{D_\alpha} - C_{L_o}\right) - mg/q_\infty \\ 0 & 0 & -S\left(C_{L_\alpha} + C_{D_o}\right) \\ 0 & 0 & -ScC_{m_\alpha} \end{bmatrix} \tag{17}$$

and

$$\left[A_{s_1}\right]_{\text{sym}} =$$

$$\begin{bmatrix} \dfrac{2S\left(C_{D_u} + C_{D_o}\right)}{(c/2)} & \dfrac{S\left(C_{D_\alpha} - C_{L_o}\right)}{(c/2)} & \dfrac{-0.5Sc\left(C_{D_{\dot\alpha}} + C_{D_q}\right)}{(c/2)} \\ \dfrac{2S\left(C_{L_u} + C_{L_o}\right)}{(c/2)} & \dfrac{S\left(C_{L_\alpha} + C_{D_o}\right)}{(c/2)} & \dfrac{-0.5Sc\left(C_{L_{\dot\alpha}} + C_{L_q}\right)}{(c/2)} \\ \dfrac{2S\left(C_{m_u} + C_{m_o}\right)}{(c/2)} & \dfrac{ScC_{m_\alpha}}{(c/2)} & \dfrac{-0.5Sc^2\left(C_{m_{\dot\alpha}} + C_{m_q}\right)}{(c/2)} \end{bmatrix} \tag{18}$$

where S and c are the reference area and chord used in the aeroelastic formulation; C_{D_u}, C_{L_u}, and C_{m_u} are the nondimensional drag, lift, and pitch moment stability derivatives, with respect to the change of the forward flight speed; C_{D_o}, C_{L_o}, and C_{m_o} are the nondimensional drag, lift, and pitch moment coefficients, at the trim condition; C_{D_α}, C_{L_α}, and C_{m_α} are the nondimensional drag, lift, and pitch moment stability derivatives, with respect to the angle of attack in radians; and $C_{D_{\dot\alpha}} + C_{D_q}$, $C_{L_{\dot\alpha}} + C_{L_q}$, and $C_{m_{\dot\alpha}} + C_{m_q}$ are the damping derivatives of the drag, lift, and pitch moment coefficients where q is the nondimensional pitch rate defined as $q = Qc/2V_\infty$ and Q is the pitch rate in rad/s.

Note that the $C_{D_u} + C_{D_o}$, $C_{L_u} + C_{L_o}$, and $C_{m_u} + C_{m_o}$ coefficients that appear in the first column of the $[A_{s_1}]_{\text{sym}}$ submatrix are the nondimensional aerodynamic stability coefficients mainly involved in the phugoid mode, but they cannot be computed accurately by

the panel methods (ZONA6[9] and doublet lattice method,[14] among others). Accordingly, to achieve a more accurate description of the aircraft dynamic behavior, the designer must replace these coefficients in the related elements of the $[A_{s_1}]_{\text{sym}}$ matrix.

At this point, a breakthrough in the RFA modeling setup is proposed to allow for both flight dynamics and aeroelastic disciplines to be handled within the unified aeroelastic modeling framework. To this end, gravity-related terms are sought to be included in the $[A_0]$ matrix, whereas the only allowable rigid-body acceleration aerodynamic derivative terms (i.e., the ones related to the $\dot{w}$ and $\dot{v}$) will be accessed through the generic $[A_2]$ matrix. Note that these are the only acceleration terms retained in the quasi-steady flight dynamic equations of motion to account for the effect on the tail of the wing/body downwash and sidewash.[11] Then, Eq. (17) clearly shows the inclusion of the gravity-related term, $-mg/q_\infty$, into the $[A_{s_0}]_{\text{sym}}$ matrix, and it will play a key role in the traditional longitudinal dynamics setup to accurately predict the phugoid mode. Additionally, there are others terms in the $[A_{s_2}]_{\text{sym}}$ submatrix that could provide some important contributions to the phugoid dynamic mode. They are identified in the second column of the $[A_{s_2}]_{\text{sym}}$ submatrix, as shown in Eq. (19):

$$\left[A_{s_2}\right]_{\text{sym}} = \begin{bmatrix} a_{11} & \dfrac{0.5ScC_{D\dot{\alpha}}}{(c/2)} & a_{13} \\ a_{21} & \dfrac{0.5ScC_{L\dot{\alpha}}}{(c/2)} & a_{23} \\ a_{31} & \dfrac{0.5Sc^2C_{m\dot{\alpha}}}{(c/2)^2} & a_{33} \end{bmatrix} \tag{19}$$

Clearly, these terms are used to facilitate the inclusion of related vertical acceleration aerodynamic stability derivative terms $\dot{w}$ into the otherwise quasi-steady longitudinal dynamic.

In a similar fashion to the symmetric case, for the three antisymmetric modes (the lateral translation, roll, and yaw modes), the submatrices in $[A_{s_0}]$ and $[A_{s_1}]$ can be correlated with the static and damping lateral nondimensional aerodynamic stability derivatives, as shown in Eqs. (20) and (21):

$$\left[A_{s_0}\right]_{\substack{\text{anti}\\ \text{sym}}} = \begin{bmatrix} 0 & mg/q_\infty & -SC_{y_\beta} \\ 0 & 0 & +SbC_{l_\beta} \\ 0 & 0 & +SbC_{n_\beta} \end{bmatrix} \tag{20}$$

$$\left[A_{s_1}\right]_{\substack{\text{anti}\\ \text{sym}}} = \begin{bmatrix} \dfrac{-SC_{y_\beta}}{(c/2)} & \dfrac{+0.5SbC_{y_p}}{(c/2)} & \dfrac{-0.5Sb}{(c/2)}\left(C_{y_{\dot{\beta}}} - C_{y_r}\right) \\ \dfrac{+SbC_{l_\beta}}{(c/2)} & \dfrac{-0.5Sb^2C_{l_p}}{(c/2)} & \dfrac{-0.5Sb^2}{(c/2)}\left(-C_{l_{\dot{\beta}}} + C_{l_r}\right) \\ \dfrac{+SbC_{n_\beta}}{(c/2)} & \dfrac{-0.5Sb^2C_{n_p}}{(c/2)} & \dfrac{-0.5Sb^2}{(c/2)}\left(-C_{n_{\dot{\beta}}} + C_{n_r}\right) \end{bmatrix} \tag{21}$$

where b, C_{y_β}, C_{l_β}, and C_{n_β} are the reference length, the nondimensional side force, roll moment, and yaw moment stability derivatives, with respect to sideslip angle in radians; C_{y_p}, C_{l_p}, and C_{n_p} are the nondimensional side force, roll moment, and yaw moment stability derivatives, with respect to the nondimensional roll rate p, where $p = Pb/2V$ and P is the roll rate in rad/s; and $C_{y_{\dot{\beta}}} + C_{y_r}$, $C_{l_{\dot{\beta}}} + C_{l_r}$, and $C_{n_{\dot{\beta}}} + C_{n_r}$ are the nondimensional damping derivatives of the side force, roll moment, and yaw moment, respectively. For accurate control modeling purposes, the nondimensional control surface aerodynamic stability derivatives can be related to the $(n_s + i)$th column and the first three rows of the $[A_0]$ and $[A_1]$ matrices, where ith represents the ith control surface. For symmetric modes, the corresponding static and damping nondimensional derivatives in the $[A_0]$ and $[A_1]$ matrices are

$$\left[A_{c_0}\right]_{\text{sym}} = \begin{bmatrix} -SC_{D_\delta} \\ -SC_{L_\delta} \\ -cSC_{m_\delta} \end{bmatrix} \in \mathbb{R}^3, \qquad \left[A_{c_1}\right]_{\text{sym}} = \begin{bmatrix} \dfrac{-0.5cSC_{D_{\dot{\delta}}}}{(c/2)} \\ \dfrac{-0.5cSC_{L_{\dot{\delta}}}}{(c/2)} \\ \dfrac{-0.5c^2SC_{m_{\dot{\delta}}}}{(c/2)} \end{bmatrix} \in \mathbb{R}^3 \tag{22}$$

where C_{D_δ}, C_{L_δ}, and C_{m_δ} are the nondimensional drag force, lift force, and pitch moment coefficients due to control surface deflection in radians and $C_{D_{\dot{\delta}}}$, $C_{L_{\dot{\delta}}}$, and $C_{m_{\dot{\delta}}}$ are the nondimensional drag, lift, and pitch moment damping derivatives due to the rate of the control surface deflection. Likewise, for antisymmetric modes, the corresponding stability derivatives in the $[A_0]$ and $[A_1]$ matrices are

$$\left[A_{c_0}\right]_{\substack{\text{anti}\\ \text{sym}}} = \begin{bmatrix} -SC_{y_\delta} \\ -SbC_{l_\delta} \\ -SbC_{n_\delta} \end{bmatrix} \in \mathbb{R}^3, \qquad \left[A_{c_1}\right]_{\substack{\text{anti}\\ \text{sym}}} = \begin{bmatrix} \dfrac{-0.5bSC_{y_{\dot{\delta}}}}{(c/2)} \\ \dfrac{-0.5b^2SC_{l_{\dot{\delta}}}}{(c/2)} \\ \dfrac{-0.5b^2SC_{n_{\dot{\delta}}}}{(c/2)} \end{bmatrix} \in \mathbb{R}^3 \tag{23}$$

Again, if C_{l_δ}, C_{n_δ}, $C_{l_{\dot{\delta}}}$, and $C_{n_{\dot{\delta}}}$ are defined in the stability axes, their signs must be reversed in accordance with Fig. 2 when they are included in ZAERO.[9] For the whole aircraft structural model containing all six translational and rotational rigid-body modes, the size of the rigid-body submatrices in $[A_{s_0}]$, $[A_{s_1}]$, and $[A_{s_2}]$ is 6×6. They are built up by combining the related rows and columns from their corresponding symmetric and antisymmetric 3×3 matrices. For instance, the $[A_{s_0}]$ matrix becomes

$$\left[A_{s_0}\right]_{\text{whole}} = \begin{bmatrix} 0 & 0 & 0 & 0 & -S\left(C_{D_\alpha} - C_{L_o}\right) - mg/q_\infty & 0 \\ 0 & 0 & 0 & mg/q_\infty & 0 & -SC_{y_\beta} \\ 0 & 0 & 0 & 0 & -S\left(C_{L_\alpha} + C_{D_o}\right) & 0 \\ 0 & 0 & 0 & 0 & 0 & -SbC_{l_\beta} \\ 0 & 0 & 0 & 0 & -ScC_{m_\alpha} & 0 \\ 0 & 0 & 0 & 0 & 0 & -SbC_{n_\beta} \end{bmatrix}_{6\times 6} \tag{24}$$

Similarly, by combining Eqs. (18) and (21), the $[A_{s_1}]_{\text{whole}}$ matrix is generated. In this manner, the aeroelastic system of Eq. (7) is now reformulated using this updated RFA setup that already included the gravity components vector, vertical-acceleration-related aerodynamic stability derivatives, and the lift and drag forces due to perturbed forward speed. Hence, a flight-dynamic-oriented rational functional approximation matrix, $[Q_{\text{FD}}(p)]$, is built up from the individual matrices described in Eqs. (17) through (23). Now, the unified aeroelastic and flight dynamics state–space description is achieved, as defined by Eq. (25):

$$\{\dot{x}_{\text{ae}}\} = [\bar{A}_{\text{ae}}]\{x_{\text{ae}}\} + [\bar{B}_{\text{ae}}]\{u\} \tag{25}$$

where $[\bar{A}_{\text{ae}}]$ and $[\bar{B}_{\text{ae}}]$ matrices are obtained through the RFA of $[Q_{\text{FD}}(p)]$. Clearly, four possible aeroelastic analysis scenarios could be built using the unified aeroelastic formulation in accordance with the aerodynamic model used and whether the elastic modes are included, as shown in Table 1. Among them, the full-frequency flight dynamic model needs to be defined. It is the aeroelastic

Table 1 Unified aeroelastic formulation—possible analysis scenarios

	Elastic modes	
Forces	Omitted	Included
Quasi-steady	Flight dynamics model	Quasisteady aeroelastic model
Unsteady	Full-frequency flight dynamics model	Full aeroelastic model

model that results when only translational and rotational rigid-body modes and the full unsteady aerodynamic model are considered. In this particular case, the rigid-body modes will be subjected to the high-frequency unsteady aerodynamic effects coming from the aerodynamic-lag-model approximation.

Finally, to avoid numerical discontinuities in the computed unsteady aerodynamic forces using the user's set of nondimensional aerodynamic-stability derivatives; a double-matching process in ZAERO[9] is devised. Technically, the aerodynamic derivative set is first used to replace the coefficients associated with the translational and rotational rigid-body modes in the generalized aerodynamic-force matrix computed in the reduced-frequency domain. Once the RFA matrices are computed in the time domain, the user's set of nondimensional static, damping, and acceleration-related derivatives is included again into the $[A_0]$, $[A_1]$, and $[A_2]$ matrices. In other words, the differences between the ZAERO-computed stability and control derivatives and the user's supplied set at zero and low-reduced-frequency values are added up to the generalized aerodynamic forces at other frequencies to assure their continuous variation with regard to the reduced-frequency range. This technique is sought to minimize the risk of jump discontinuities in any of the elements that compose the matrix $[Q_{\mathrm{FD}}(p)]$.

V. Longitudinal and Lateral Dynamics: Closed-Form Solutions

Closed-form solutions are computed using MATHEMATICA software[15] for symmetric and antisymmetric rigid-body maneuvers with the unified aeroelastic formulation to emulate those ordinarily used by the flight dynamic engineer (i.e., separate longitudinal and lateral dynamic behavior analysis).[11] Specifically, the longitudinal dynamic equations of motion, without considering any additional elastic modes in the model, are obtained in closed form by incorporating Eqs. (17) to (19) and (22) into Eq. (3) while applying the similarity transformation $[T_A]_{\mathrm{long}}$; that is,

$$\dot{x}_{\mathrm{long}} = \underbrace{\left[T_A^{-1}\bar{A}_{\mathrm{ae}}T_A\right]_{\mathrm{long}}}_{A_{\mathrm{long}}} x_{\mathrm{long}} + \underbrace{\left[T_A^{-1}\bar{B}_{\mathrm{ae}}\right]_{\mathrm{long}}}_{B_{\mathrm{long}}} u_{\mathrm{long}}$$

$$x_{\mathrm{long}}^T = \{x \quad u \quad h \quad w \quad \theta \quad q\}^T, \qquad u_{\mathrm{long}} = \delta_e \tag{26}$$

where x, u, h, w, θ, q, and δ_e are the perturbed forward displacement, forward airspeed, altitude, upward velocity, Euler pitch angle, pitch rate, and the elevator control surface deflection angle, respectively. After neglecting the first and third rows and columns related to the perturbed forward displacement and altitude airframe states, x and h, we proceed to evaluate each nonzero element of the transformed dynamic matrix $[T_A^{-1}\bar{A}_{\mathrm{ae}}T_A]_{\mathrm{long}}$ along its columns.

column 1:

$$\left[T_A^{-1}\bar{A}_{\mathrm{ae}}T_A(1,1)\right]_{\mathrm{long}} = -\frac{2q_\infty S\left(C_{D_0}+C_{D_u}\right)}{mV_\infty} \triangleq X_u$$

$$\left[T_A^{-1}\bar{A}_{\mathrm{ae}}T_A(2,1)\right]_{\mathrm{long}} = -\frac{2q_\infty S\left(C_{L_0}+C_{L_u}\right)}{mV_\infty} \triangleq Z_u$$

$$\left[T_A^{-1}\bar{A}_{\mathrm{ae}}T_A(4,1)\right]_{\mathrm{long}} = -\frac{q_\infty Sc\left[2mV_\infty^2\left(C_{m_0}+C_{m_u}\right)-q_\infty Sc\left(C_{L_0}+C_{L_u}\right)C_{m_{\dot{\alpha}}}\right]}{mV_\infty^3 I_{yy}} \triangleq \left(M_u + M_{\dot{w}}Z_u\right)$$

column 2:

$$\left[T_A^{-1}\bar{A}_{\mathrm{ae}}T_A(1,2)\right]_{\mathrm{long}} = -\frac{q_\infty S\left(C_{D_\alpha}-C_{L_0}\right)}{mV_\infty} \triangleq X_w$$

$$\left[T_A^{-1}\bar{A}_{\mathrm{ae}}T_A(2,2)\right]_{\mathrm{long}} = -\frac{q_\infty S\left(C_{D_0}+C_{L_\alpha}\right)}{mV_\infty} \triangleq Z_w$$

$$\left[T_A^{-1}\bar{A}_{\mathrm{ae}}T_A(4,2)\right]_{\mathrm{long}} = -\frac{q_\infty Sc\left[-2mV_\infty^2 C_{m_\alpha}+q_\infty Sc\left(C_{D_0}+C_{L_\alpha}\right)C_{m_{\dot{\alpha}}}\right]}{2mV_\infty^3 I_{yy}} \triangleq \left(M_w + M_{\dot{w}}Z_w\right)$$

column 3:

$$\left[T_A^{-1}\bar{A}_{\mathrm{ae}}T_A(1,3)\right]_{\mathrm{long}} = -g$$

column 4:

$$\left[T_A^{-1}\bar{A}_{\mathrm{ae}}T_A(1,4)\right]_{\mathrm{long}} = -\frac{q_\infty Sc\left(C_{D_q}+C_{D_{\dot{\alpha}}}\right)}{2mV_\infty} \triangleq X_{\dot{w}}$$

$$\left[T_A^{-1}\bar{A}_{\mathrm{ae}}T_A(2,4)\right]_{\mathrm{long}} = V_\infty - \frac{q_\infty Sc\left(C_{L_q}+C_{L_{\dot{\alpha}}}\right)}{2mV_\infty} \triangleq \left(V_\infty + Z_q\right)$$

$$\left[T_A^{-1}\bar{A}_{\mathrm{ae}}T_A(3,4)\right]_{\mathrm{long}} = 1$$

$$\left[T_A^{-1}\bar{A}_{\mathrm{ae}}T_A(4,4)\right]_{\mathrm{long}} = \frac{q_\infty Sc^2\left\{2mV_\infty^2 C_{m_q}+\left[2mV_\infty^2-q_\infty Sc\left(C_{L_q}+C_{L_{\dot{\alpha}}}\right)\right]C_{m_{\dot{\alpha}}}\right\}}{2mV_\infty^3 I_{yy}} \triangleq \left[M_q + M_{\dot{w}}\left(V_\infty + Z_q\right)\right]$$

as well as the input vector $\{T_A^{-1}\bar{B}_{\mathrm{ae}}\}_{\mathrm{long}}$:

column 1:

$$\left\{T_A^{-1}\bar{B}_{\mathrm{ae}}(1,1)\right\}_{\mathrm{long}} = \frac{q_\infty S\left(-C_{D_\delta}\right)}{m} \triangleq X_{\delta_e}$$

$$\left\{T_A^{-1}\bar{B}_{\mathrm{ae}}(2,1)\right\}_{\mathrm{long}} = \frac{q_\infty S\left(-C_{L_\delta}\right)}{m} \triangleq Z_{\delta_e}$$

$$\left\{T_A^{-1}\bar{B}_{\mathrm{ae}}(4,1)\right\}_{\mathrm{long}} = \frac{-q_\infty Sc\left[-2mV_\infty^2 C_{m_\delta}+q_\infty ScC_{L_\delta}C_{m_{\dot{\alpha}}}\right]}{2mV_\infty^2 I_{yy}} \triangleq \left(M_{\delta_e} + M_{\dot{w}}Z_{\delta_e}\right)$$

where the variables X_u, X_w, and so forth are defined in accordance to Table 4.3 of Ref. 11. It is observed that the resulting state–space representation accurately recovers the classical form of the longitudinal dynamics referenced to stability axes as shown in Eq. (27):

$$\begin{Bmatrix} \dot{u} \\ \dot{w} \\ \dot{\theta} \\ \dot{q} \end{Bmatrix} = \begin{bmatrix} X_u & X_w & -g & 0 \\ Z_u & Z_w & 0 & (V_\infty + Z_q) \\ 0 & 0 & 0 & 1 \\ (M_u + M_{\dot{w}}Z_u) & (M_w + M_{\dot{w}}Z_w) & 0 & (M_q + M_{\dot{w}}(V_\infty + Z_q)) \end{bmatrix}$$

$$\times \begin{Bmatrix} u \\ w \\ \theta \\ q \end{Bmatrix} + \begin{Bmatrix} X_{\delta_e} \\ Z_{\delta_e} \\ 0 \\ \left(M_{\delta_e} + M_{\dot{w}} Z_{\delta_e}\right) \end{Bmatrix} \delta_e \tag{27}$$

The longitudinal stability quartic is then computed from

$$\det(sI - A_{\text{long}}) = 0 \tag{28}$$

and its solution, in the most general case, will be composed with both free longitudinal oscillatory modes, that is, the short-period and the phugoid modes.

The closed-form lateral equations of motion are computed in a similar fashion as in the longitudinal dynamics case. Thus, Eqs. (20), (21), and (23) are fed into Eq. (3), and by applying the similarity transformation $[T_A]_{\text{lat}}$, the lateral equations are

$$\dot{x}_{\text{lat}} = [A]_{\text{lat}} x_{\text{lat}} + [B]_{\text{lat}} u_{\text{lat}}$$

$$x_{\text{lat}}^T = \{y \quad \beta \quad p \quad r \quad \phi \quad \psi\}^T, \qquad u_{\text{lat}}^T = \{\delta_a \quad \delta_r\}^T \tag{29}$$

where y, β, p, r, ϕ, ψ, δ_a, and δ_r are the perturbed lateral displacement, sideslip angle, roll rate, yaw rate, Euler roll angle, Euler yaw angle, and aileron and rudder control surface deflection angle, respectively.

The first and last rows and columns related to the perturbed lateral displacement and yaw-angle states, y and ψ, are eliminated. As before, we evaluate each nonzero element of the transformed dynamic matrix $[T_A^{-1} \bar{A}_{\text{ae}} T_A]_{\text{lat}}$ along its columns.

column 1

$$\left[T_A^{-1} \bar{A}_{\text{ae}} T_A(1,1)\right]_{\text{lat}} = \frac{q_\infty S C_{y_\beta}}{m V_\infty} \triangleq Y_v$$

$$\left[T_A^{-1} \bar{A}_{\text{ae}} T_A(2,1)\right]_{\text{lat}} = -\frac{q_\infty b S\left(C_{n_\beta} I_{xz} + C_{l_\beta} I_{zz}\right)}{I_{xz}^2 - I_{xx} I_{yy}}$$

$$= \frac{\left(L_\beta + N_\beta I_{xz}/I_{xx}\right)}{\left(1 - I_{xz}^2/I_{xx} I_{zz}\right)} \triangleq L'_\beta$$

$$\left[T_A^{-1} \bar{A}_{\text{ae}} T_A(3,1)\right]_{\text{lat}} = -\frac{q_\infty b S\left(C_{n_\beta} I_{xx} + C_{l_\beta} I_{xz}\right)}{I_{xz}^2 - I_{xx} I_{yy}}$$

$$= \frac{\left(N_\beta + L_\beta I_{xz}/I_{zz}\right)}{\left(1 - I_{xz}^2/I_{xx} I_{zz}\right)} \triangleq N'_\beta$$

column 2

$$\left[T_A^{-1} \bar{A}_{\text{ae}} T_A(1,2)\right]_{\text{lat}} = \frac{q_\infty b S C_{y_p}}{2 m V_\infty^2} \triangleq Y_p^*$$

$$\left[T_A^{-1} \bar{A}_{\text{ae}} T_A(2,2)\right]_{\text{lat}} = -\frac{q_\infty b^2 S\left(C_{n_p} I_{xz} + C_{l_p} I_{zz}\right)}{2 V_\infty \left(I_{xz}^2 - I_{xx} I_{zz}\right)}$$

$$= \frac{\left(L_p + N_p I_{xz}/I_{xx}\right)}{\left(1 - I_{xz}^2/I_{xx} I_{zz}\right)} \triangleq L'_p$$

$$\left[T_A^{-1} \bar{A}_{\text{ae}} T_A(3,2)\right]_{\text{lat}} = -\frac{q_\infty b^2 S\left(C_{n_p} I_{xx} + C_{l_p} I_{xz}\right)}{2 V_\infty \left(I_{xz}^2 - I_{xx} I_{zz}\right)}$$

$$= \frac{\left(N_p + L_p I_{xz}/I_{zz}\right)}{\left(1 - I_{xz}^2/I_{xx} I_{zz}\right)} \triangleq N'_p$$

$$\left[T_A^{-1} \bar{A}_{\text{ae}} T_A(4,2)\right]_{\text{lat}} = 1$$

column 3

$$\left[T_A^{-1} \bar{A}_{\text{ae}} T_A(1,3)\right]_{\text{lat}} = \frac{q_\infty b S\left(C_{y_r} - C_{y_{\dot{\beta}}}\right)}{2 m V_\infty^2} - 1 \triangleq \left(Y_r^* - 1\right)$$

$$\left[T_A^{-1} \bar{A}_{\text{ae}} T_A(2,3)\right]_{\text{lat}} = -\frac{q_\infty b^2 S\left[\left(C_{n_r} - C_{n_{\dot{\beta}}}\right) I_{xz} + \left(C_{l_r} - C_{l_{\dot{\beta}}}\right) I_{zz}\right]}{2 V_\infty \left(I_{xz}^2 - I_{xx} I_{zz}\right)}$$

$$= \frac{\left(L_r + N_r I_{xz}/I_{xx}\right)}{\left(1 - I_{xz}^2/I_{xx} I_{zz}\right)} \triangleq L'_r$$

$$\left[T_A^{-1} \bar{A}_{\text{ae}} T_A(3,3)\right]_{\text{lat}} = -\frac{q_\infty b^2 S\left[\left(C_{n_r} - C_{n_{\dot{\beta}}}\right) I_{xx} + \left(C_{l_r} - C_{l_{\dot{\beta}}}\right) I_{xz}\right]}{2 V_\infty \left(I_{xz}^2 - I_{xx} I_{zz}\right)}$$

$$= \frac{\left(N_r + L_r I_{xz}/I_{zz}\right)}{\left(1 - I_{xz}^2/I_{xx} I_{zz}\right)} \triangleq N'_r$$

column 4

$$\left[T_A^{-1} \bar{A}_{\text{ae}} T_A(1,4)\right]_{\text{lat}} = g/V_\infty$$

where the variables Y_v, Y_p^*, and so forth are defined in accordance to Table 4.3 of Ref. 11. The resulting state–space representation is able to retrieve the traditional lateral dynamics as shown in Eq. (30):

$$\begin{Bmatrix} \dot{\beta} \\ \dot{p} \\ \dot{r} \\ \dot{\phi} \end{Bmatrix} = \begin{bmatrix} Y_v & Y_p^* & \left(Y_r^* - 1\right) & g/V_\infty \\ L'_\beta & L'_p & L'_r & 0 \\ N'_\beta & N'_p & N'_r & 0 \\ 0 & 1 & 0 & 0 \end{bmatrix} \begin{Bmatrix} \beta \\ p \\ r \\ \phi \end{Bmatrix} + \begin{bmatrix} Y_{\delta_a}^* & Y_{\delta_r}^* \\ L'_{\delta_a} & L'_{\delta_r} \\ N'_{\delta_a} & N'_{\delta_r} \\ 0 & 0 \end{bmatrix} \begin{Bmatrix} \delta_a \\ \delta_r \end{Bmatrix} \tag{30}$$

As in the longitudinal case, the solution of the lateral characteristic equation

$$\det(sI - A_{\text{lat}}) = 0 \tag{31}$$

will generate the free lateral dynamic modes. These consist of three modes; they are the roll subsidence, the spiral, and the Dutch-roll modes.

Clearly, Eqs. (27) and (30) indicate that both plane dynamic equations of motion are fully recovered from the unified aeroelastic formulation, when no elastic modes are considered in addition to the set of rigid-body modes. This is neatly accomplished by taking advantage of the inherent flight dynamic modeling capabilities provided by the RFA framework.

VI. Application Examples

For numerical comparison purposes a case study is developed using a realistic model as the full aeroelastic GA-ASI Predator UAV®.[8] It is used to evaluate the effects on the classical longitudinal and lateral dynamic modes caused by the inclusion of several elastic modes into the aeroelastic model. This example illustrates the application of the present methodology using standard production flutter-analysis tools, and it is implemented using ZAERO/ASE[9] as well as the MATLAB®/Simulink environment.[16]

Case Study: Predator UAV

The Predator is a UAV that is used for medium-altitude endurance observation and was developed by GA-ASI in 1994. The Predator is a pusher-type design (rear-mounted Rotax-powered engine/propeller), with a composite airframe and a retractable tricycle landing gear. The fuel stores and all payloads are mounted within the fuselage. The overall vehicle length is 8.23 m (27 ft), with a wingspan of 14.84 m (48.7 ft). The wing has large inboard flaps for varying wing lift and large outboard ailerons for vehicle roll control. The vehicle performance specifications include operational altitudes of more than 7500 m (25,000 ft), endurance of more than 24-h flight at 740 km (400 nm), a sea-level cruise-speed range of

Table 2 Predator UAV rigid-body dynamics: quasi-steady aerodynamic model and number of elastic modes

		RFA: Quasi-steady aerodynamic modes		
Dynamic modes	Traditional flight dynamics	Rigid-body modes only	Rigid-body + 1 elastic mode	Rigid-body + 6 Elastic modes
Short-period	$-0.0151 \pm j\ 0.1178$	$-0.0151 \pm j\ 0.1178$	$-0.0173 \pm j\ 0.1166$	$+0.0325 \pm j\ 0.0825$
Phugoid #1	-2.2943	-2.2941	-2.4740	-2.4707
Phugoid #2	-1.1587	-1.1588	-1.1367	-1.1794
Roll subsidence	-8.3781	-8.3720	-8.3731	-8.7319
Dutch roll	$-0.2804 \pm j\ 1.2266$	$-0.2804 \pm j\ 1.2266$	$-0.2804 \pm j\ 1.2266$	$-0.2772 \pm j\ 1.2557$
Spiral	$+0.0544$	$+0.0544$	$+0.0544$	$+0.0586$

Table 3 Predator UAV rigid-body dynamics: unsteady aerodynamic model and number of elastic modes

		RFA: Unsteady aerodynamic modes		
Aeroelastic modes	Traditional flight dynamics	Rigid-body modes only	Rigid-body + 1 elastic mode	Rigid-body + 6 elastic modes
1, 2	$-0.0151 \pm j\ 0.1178$	$0.0191 \pm j\ 0.1081$	$-2.2537 \pm j\ 1.0601$	$-1.9133, -2.7929$
3	-2.2943	-3.0372	$+0.0119$	$+0.0130$
4	-1.1587	-1.2078	$+0.7787$	$+0.4149$
5	-8.3781	-10.722	-11.623	-8.6448
6, 7	$-0.2804 \pm j\ 1.2266$	$-0.1851 \pm j\ 1.1372$	$-0.2163 \pm j\ 1.1849$	$-0.2721 \pm j\ 1.2159$
8	$+0.0544$	$+0.03257$	$+0.0397$	$+0.05742$

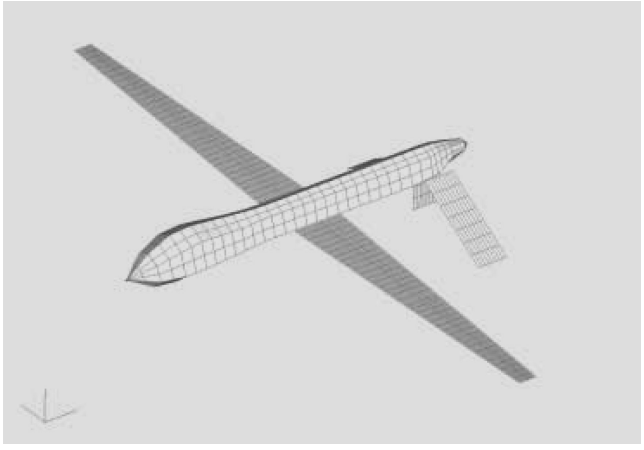

Fig. 4 GA-ASI Predator UAV.

178–220 km/h (96–120 kn), and a sea-level dive speed of 278 km/h (151 kn), respectively.

The aeroelastic model for the whole aircraft was created using the NASTRAN and ZAERO[9] software systems. The aerodynamic forces in the frequency domain were computed through ZONA6, ZAERO's subsonic unsteady aerodynamic method, and its time domain realization was performed using the minimum-state approach[10,13] implemented by the ZAERO/ASE module. The aeroelastic model includes 13 elastic structural modes with frequency content up to 10.3 Hz in addition to the complete set of rigid-body modes. A detailed set of static, damping, and translational acceleration-related nondimensional stability derivatives are available to the flight control designer, and this database is used to update the quasi-steady aerodynamic matrices $[A_0]$, $[A_1]$, and $[A_2]$ in $[Q_{\mathrm{FD}}(p)]$. Figure 4 shows the employed Predator UAV aerodynamic model.

In what follows, the influence of the aerodynamic model and the number of elastic modes on the translational and rotational UAV's rigid-body dynamic behavior is analyzed. Table 2 presents the effects on the dynamic modes, noted in the first column, when a quasi-steady aerodynamic model is employed; that is $E_s = E_c = \bar{R} = \bar{D} = \bar{M}_c \triangleq 0$ in Eq. (6). The results presented in the second column are obtained using traditional flight dynamic equations,[11] whereas the values in the other columns are computed through the unified aeroelastic formulation. The first column under the RFA portion only considers the set of translational and rotational rigid-body modes, whereas the second and third columns under the RFA portion have added one and six structural elastic modes, respectively. In this case, all included elastic modes are wing-bending modes.

Clearly, the updated quasi-steady model with no elastic modes (first column under the RFA) accurately recovers the traditional flight dynamic results. In contrast, the quasi-steady aeroelastic model generated by the inclusion of a set of elastic modes (see Table 1) strongly affects the longitudinal dynamics. Specifically the damping and frequency of the short-period mode changed with the addition of one elastic mode, and ultimately the mode becomes unstable when six elastic modes are used. As expected, the lateral dynamic modes, that is, the roll subsidence, Dutch roll, and spiral, are practically unaffected by the wing-bending modes. Hence, the usual separation assumption between the longitudinal and lateral dynamic is clearly preserved through the unified aeroelastic formulation.

Now, the modified UAV rigid-body dynamics caused by the use of the full unsteady aerodynamic model and the inclusion of different numbers of elastic modes are shown in Table 3. In the first column, the dynamic modes of Table 2 are renamed as aeroelastic modes, and the second column is preserved for comparative purposes during the following discussions. The columns under the RFA portion indicate a noticeable influence of the flow unsteadiness on the translational and rotational rigid-body dynamics, even when elastic modes are not taken into account. These high-reduced-frequency unsteady aerodynamic effects are modeled in the full-frequency flight dynamic model (see Table 1) through the E_s, E_c, $\bar{R}$, $\bar{D}$, and $\bar{M}_c$ matrices in the aeroelastic state–space description of Eq. (6). As before, the added elastic modes have clearly affected those aeroelastic modes resembling longitudinal dynamics. In particular, the first column under the RFA portion shows that the first and second aeroelastic modes, supposedly related with the short-period dynamic, become unstable. These particular modes keep changing their qualitative dynamic behavior as a function of the number of elastic modes considered in the UAV model, going from divergent to convergent oscillatory modes and finally becoming a pair of stable decaying modes. Similarly, the third and fourth aeroelastic modes changed their stability behavior.

It is quite interesting that as the number of elastic modes is increased, the aeroelastic modes 5–8 become comparable to the classical lateral dynamic modes noted in the first column, that is, the roll-subsidence, Dutch-roll, and spiral modes, respectively. In fact, this finding can presumably be used to lay out a practical criterion to determine the approximate number of elastic modes that need to be included in the aeroelastic model to accurately model its flight dynamic behavior. For instance, if only symmetric (antisymmetric) maneuvers are performed, a trade-off between the numbers of symmetric (antisymmetric) elastic modes vs the accurate recovery of the traditional lateral (longitudinal) dynamics can easily be

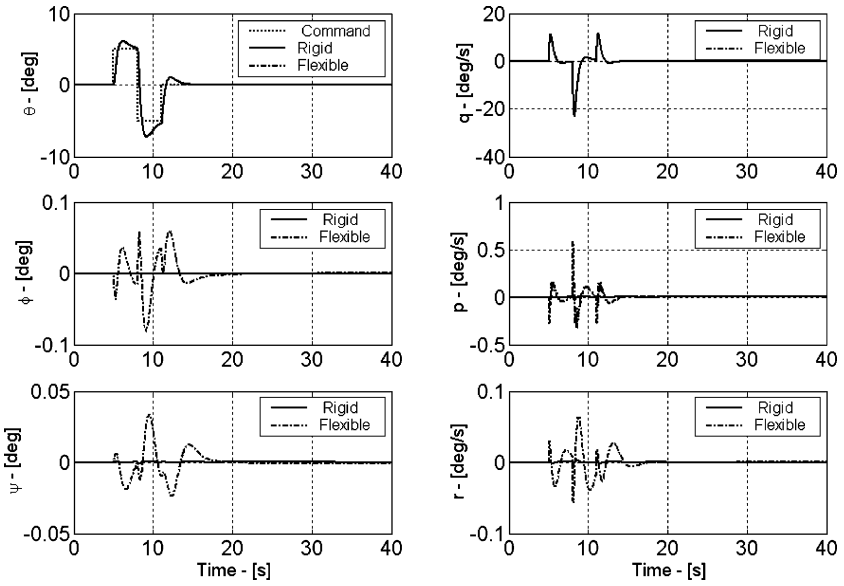

Fig. 5 Predator UAV: closed-loop state vector variables.

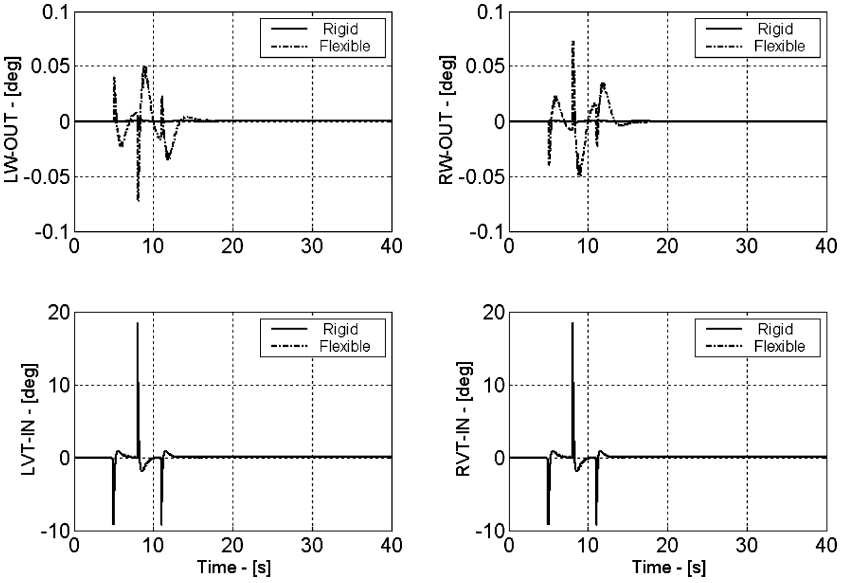

Fig. 6 Predator UAV: closed-loop control variables.

implemented by the flight control designer using the proposed aeroelastic formulation.

Finally, Figs. 5 and 6 show the time trace responses of the state and control vectors for the coupled aeroelastic Predator UAV model to a symmetric doublet applied in the pitch command channel when six elastic modes are included. Initially, a preliminary flight controller, with weakly coupled longitudinal and lateral feedback control using angular rates as inner loops, is designed to deal with a quasi-steady flight dynamic model (rigid-body models only). In this design, the coupling came from the Predator "A" tail configuration used to control both longitudinal and lateral/directional planes.

It can be observed from Fig. 5 that the addition of the six wing-related elastic modes negligibly modified the Predator's closed-loop longitudinal responses, that is, $\theta(t)$ and $q(t)$ (not visible to the naked eye).In contrast, the lateral/directional variable responses, that is, $\phi(t)$, $\psi(t)$, $p(t)$, and $r(t)$, are noticeably affected by the aeroelastic effects. The closed-loop control variables, depicted in Fig. 6, also show some differences when the aeroelastic model is considered in place of the quasi-steady flight dynamic model. An increase in the left and right aileron activities for the aeroelastic model, through the wing-aileron control variables LW-OUT and RW-OUT, is visible in the upper portion of Fig. 6. In contrast, its lower portion did not show substantial differences in the left and right vertical tail control surfaces (LVT-IN and RVT-IN time traces). Consequently, these results confirm the use of the unified aeroelastic formulation as an enabling tool to take into account the influence of aeroelastic effects on the translational and rotational behavior of the Predator UAV.

VII. Summary

In this paper, a unified aeroelastic formulation using the rational function approximations setup is presented to recover the longitudinal and lateral equations of motion ordinarily used by the flight control engineer. This approach sought to identify key elements within the rational function approximation to update the unsteady aerodynamic model. By allowing the inclusion of gravity components, vertical-acceleration-related aerodynamic stability derivatives, and the lift and drag forces due to forward-velocity perturbations into the rational function approximation matrices, the traditional quasi-steady flight dynamic equations of motion are recovered using the proposed unified aeroelastic formulation. We hope this modeling framework will become the aeroelastician's natural enabling tool

by providing a common state–space representation that accurately models the influence of the elastic modes on the dynamic behavior of the whole aircraft.

It is shown by closed-form solutions that quasi-steady longitudinal and lateral dynamics are exactly recovered when no elastic modes are presented in the aeroelastic model. The Predator UAV aeroelastic model is used to demonstrate the application of the unified aeroelastic framework to a realistic complex model.

Acknowledgments

The authors thank Martin Brenner of NASA Dryden Flight Research Center for his valuable discussions and feedback during the devising stage of the unified aeroelastic formulation and John Hutcheson of GA-ASI for his valuable contribution with the Predator flight dynamics. In addition, the authors thank the anonymous reviewers for their comments on the draft of this paper. Their suggestions considerably improved the final version.

References

[1]Bryson, A. E., "Control of Spacecraft and Aircraft," Princeton Univ. Press, Princeton, NJ, 1994, Chap. 15.

[2]Rodden, W. P., and Love, J. R., "Equations of Motion of a Quasisteady Flight Vehicle Utilizing Restrained Static Aeroelastic Characteristics," *Journal of Aircraft*, Vol. 22, No. 9, 1985, pp. 802–809.

[3]Winther, A. A., Hagemeyer, D. A., Britt, R. T., and Rodden, W. P., "Aeroelastic Effects on the B-2 Maneuver Response," *Journal of Aircraft*, Vol. 32, No. 4, 1995, pp. 862–867.

[4]Winther, B. A., Goggin, P. J., and Dykman, J. R., "Reduced Order Dynamic Aeroelastic Model Development and Integration with Nonlinear Simulation," *Journal of Aircraft*, Vol. 37, No. 5, 2000, pp. 833–839.

[5]Dykman, J. R., and Rodden, W., "Structural Dynamics and Quasistatic Aeroelastic Equations of Motion," *Journal of Aircraft*, Vol. 37, No. 3, 2000, pp. 538–542.

[6]Rodden, W. P., Bellinger, E. D., and Giesing, J. P., "Errata and Addenda to 'Application of Oscillatory Aerodynamic Theory to Estimation of Dynamic Stability Derivatives,'" *Journal of Aircraft*, Vol. 21, No. 1, 1984, pp. 93, 94.

[7]Lind, R., and Brenner, M., "Robust Aeroservoelastic Stability Analysis: Flight Test Applications," Springer-Verlag, London, 1999, Chap. 4.

[8]Kosmatka, J. B., and Panza, J., "Aeroelastic Analysis of a Composite Unmanned Air Vehicle," AIAA Paper 2002-1208, April 2002.

[9]ZONA Technology, "ZAERO User's Manual," Ver. 7.2, Scottsdale, AZ, Nov. 2004.

[10]Karpel, M., "Size-Reduction Techniques for the Determination of Efficient Aeroservoelastic Models," *Control and Dynamic Systems—Advances in Theory and Applications*, Vol. 54, Academic Press, San Diego, CA, 1992, pp. 263–295.

[11]McRuer, D., Ashkenas, I., and Graham, D., "Aircraft Dynamics and Automatic Control," Princeton Univ. Press, Princeton, NJ, 1990, Chaps. 4–6.

[12]Roger, K. L., "Airplane Math Modeling Methods for Active Control Design," *Proceedings of the 44th AGARD Structures and Materials Panel*, AGARD-CP-228, April 1977, pp. 4.1–4.11.

[13]Karpel, M., "Design of the Active Flutter Suppression and Gust Load Alleviation Using State-Space Aeroelastic Modeling," *Journal of Aircraft*, Vol. 19, No. 6, 1982, pp. 221–227.

[14]Albano, E., and Rodden, W. P., "A Doublet-Lattice Method for Calculating Lift Distributions on Oscillating Surfaces in Subsonic Flow," *AIAA Journal*, Vol. 7, No. 2, 1969, pp. 279–285.

[15]Wolfram, S., *Mathematica 5*, Wolfram Media, Champaign, IL, 2003.

[16]MathWorks, *MATLAB 7.0 and Simulink 6.0 User's Manual*, Natick, MA, 2004.